PROCEEDINGS, 42nd Workshop on Geothermal Reservoir Engineering
Stanford University, Stanford, California, February 13-15, 2017
SGP-TR-212

Improved PetraSim-TOUGH2 Capabilities for the Simulation of Geothermal Reservoirs

Alfredo Battistelli, Daniel Swenson and Alison Alcott

Saipem SpA, 61032 Fano (PU), Italy; Thunderhead Engineering Consultants Inc., Manhattan, KS, USA; RockWare Inc., Golden, CO, USA

alfredo.battistelli@saipem.com; swenson@thunderheadeng.com; alison@rockware.com

Keywords: TOUGH2, PETRASIM, EWASG, EOS2, reservoir simulation

ABSTRACT

A new release of PetraSim-TOUGH2 (TOUGH2P V2.0) includes updated fluid thermodynamics calculations and improvements related to flow processes and the treatment of production wells. While some of the improvements are applicable to all the TOUGH2P EOS modules supported by PetraSim 2017, the primary focus is the EOS modules customarily used for the modelling of geothermal reservoirs: EOS1 for pure water, EOS2 for water-CO_2 mixtures, and EWASG for ternary H_2O-CO_2-NaCl mixtures.

Improvements to the TOUGH2 V2 code (Pruess et al., 1999) include: the use of IAPWS-IF97 and IAPWS 2008 correlations for water and steam, additional correlations for brine and halite properties in EWASG, for EOS2 and EWASG the dependence of aqueous phase density on dissolved non-condensable gas (NCG) concentration and a modified approach to calculate the enthalpy contribution of dissolved NCG to the aqueous phase enthalpy, for EOS2 a new option for CO_2 density calculation and an updated solubility model, and improvements to numerical implementation of the van Genuchten capillary pressure function.

The PetraSim interface supports these new options. In addition, there are new capabilities for production wells that include: PI specified for each layer for wells completed on multiple layers, wells on deliverability activated at specific times, and optional input of a pre-calculated flowing wellbore pressure profile.

PetraSim-TOUGH2P applications are presented to demonstrate the use and advantages of some of the modifications included in TOUGH2P, its EOS modules and in the PetraSim pre- and post-processing interface to TOUGH2P.

1. INTRODUCTION

TOUGH2 V2 (Pruess et al., 1999) is a numerical simulator for nonisothermal flows of multicomponent, multiphase fluids in one, two, and three-dimensional porous and fractured media. It uses the "integral finite difference" method to solve the mass and energy balance equations for fluid and heat flow in multiphase, multicomponent systems.

PetraSim is an interactive graphical user interface for the TOUGH2 code family. TOUGH2P V2.0 executables are included with PetraSim. The licensing arrangement with the Department of Energy allows Thunderhead Engineering to modify and distribute the modified executables. Later versions of TOUGH2 (V2.1 and some of the specialized TOUGH2 equations of state) must be purchased directly from Lawrence Berkeley National Laboratory. As a consequence, the modifications described in this paper are based on TOUGH2 V2.

One major area of application of TOUGH2P (and PetraSim) is geothermal reservoir modeling. For geothermal applications, the most frequently used equation of state options are: EOS1 for pure water, EOS2 for water-CO_2 mixtures, and EWASG for ternary H_2O-CO_2-NaCl mixtures.

This paper describes the changes made to both TOUGH2P V2.0 and PetraSim to improve support for geothermal applications.

2. MODIFICATIONS SHARED BY ALL TOUGH2 EOS MODULES

Some modifications included in TOUGH2P V2.0 are applicable to all EOS modules, except TMVOC and T2VOC. These changes have been implemented as options, so that compatibility with previous official versions are preserved.

2.1 IAPWS thermodynamic correlations

TOUGH2 V2 (Pruess et al., 1999) uses the old IFC-67 correlations (IFC, 1967) for the computation of vapor pressure, density and internal energy of liquid water and steam. The TOUGH2 V2 limits are 350°C.

The more accurate and computationally faster IAPWS-IF97 formulation (IAPWS, 2007) was initially implemented within TOUGH2 by Croucher and O'Sullivan (2008), but was not officially released. TOUGH2P V2.0 includes IAPWS-IF97 correlations coded by Battistelli that can be chosen as an alternate to the old IFC-67. The IAPWS (2008) formulation for the dynamic viscosity of water and steam has been also implemented, with a consistent improvement of accuracy at high temperatures with respect to previous correlations (Battistelli, 2012). Even though the IAPWS-IF97 correlations are officially limited to 350°C for the liquid water, they can be safely used up to 360°C for both water and steam, and up 1400 bar for liquid water with minor errors. In EWASG module P and T up to 1400 bar and 365°C, respectively, are now allowed if IAPWS-IF97 correlations are chosen. Such high pressure might be useful for geopressured

geothermal reservoirs under single liquid conditions. If two-phase conditions are present due to the bubbling pressure of dissolved NCG, the simulation of such conditions would require a check of the accuracy of brine-NCG thermodynamic equilibrium for the specific application.

2.2 van Genuchten capillary pressure formulation

The van Genuchten (1980) formulation (VG) is frequently used to describe the capillary pressure of a two-phase system with respect to saturation of the wetting phase. The correlation is characterized by a zero entry pressure at full liquid saturated conditions which can be responsible, depending on the chosen parameters, of very large capillary pressure derivatives at the single-liquid ←→ two-phase transition, often accompanied by numerical instability and slow convergence of the Newton-Raphson (NR) iteration process. It is known that the Brooks and Corey (1966) model (BC) with a finite gas entry pressure improves the phase transition stability and for this reason it was implemented within versions of TOUGH2 V2 that were not officially released (Pruess, 2007). That implementation was made by accounting for the finite gas entry pressure in the single-liquid ←→ two-phase transition tests to maintain the continuity of aqueous phase pressure across the phase boundary. Instead of including the BC model, the existing VG model has been modified to allow the input of SLS values (the saturation at which capillary pressure is zero) greater than 1 to obtain a finite gas entry pressure without modification of phase transition tests. Checks made by running two-phase problems with both EOS2 and EWASG showed clear improvements in the simulation speed, with a smaller number of time steps and NR iterations, even without the modification of phase transition tests.

The VG model presents an asymptotic behavior for liquid saturation approaching the SLR≥0 value, which in the original VG formulation corresponds to the irreducible liquid saturation used for the relative permeability curves. To avoid this unphysical behavior Pruess et al. (1999) suggest to set SLR in the VG capillary pressure model at values lower than the SLR chosen for the relative permeability curve and provide the option to limit the capillary pressure to a maximum value chosen by the user. In the present version of subroutine PCAP, an option has been made available to use a linear extrapolation of capillary pressure to dry conditions starting at a given aqueous saturation SL and preserving at that point the function derivability. This allows a smoother and more physical behavior of capillary pressure for vanishing liquid saturations.

The capillary pressure curves implemented by TOUGH2 V2 are functions of wetting phase saturation only and do not depend on thermodynamic conditions and phases composition, apart for the Leverett (1941) model for which the capillary pressure is a function of the water-steam surface tension which declines with temperature to zero at the critical point. Scaling of laboratory capillary pressure data as function of surface tension and contact angle is a common practice in the oil and gas industry where the nitrogen-brine system is often used instead of the more challenging methane-brine system. Capabilities for capillary pressure scaling are now available if the surface tension of the two-phase mixture used at lab conditions, or at some other reference conditions (*ref*), is provided for a specific rock domain. In this case the surface tension (σ) of the water-steam, or brine-steam, two-phase mixture is computed following Battistelli (2012) and used to scale the capillary pressure value (P_c) at reservoir conditions (*res*) as follows, where T is temperature and X_S is the NaCl mass fraction in the aqueous phase:

$$P_{c,res} = P_{c,ref} \frac{\sigma_{res}(T, X_S)}{\sigma_{ref}} \qquad \text{if} \qquad \sigma_{ref} > 0 \tag{1}$$

This approximate approach both neglects the effects of NCG on surface tension (in both EOS2 and EWASG) and those of contact angle not accounted for in Eq.1. It has anyway the advantage to account for the temperature effects which might be remarkable in geothermal reservoir simulations. An example is the modeling of injection of cold recovered condensate and separated brine into a two-phase high temperature reservoir performed for production forecast simulations of geothermal reservoirs. The dependence on temperature of capillary pressure may have a remarkable effect on the migration and evaporation of injected liquids.

2.3 Wells on deliverability

Production wells discharging from multiple grid layers, common in full field geothermal simulations, can be modeled using the well on deliverability approach with each layer contributing to wellbore flow proportionally to the difference between well block pressure and local wellbore flowing pressure. Following Coats (1977), the mass rate of phase β discharged by the generic layer is given by (Pruess et al., 1999):

$$q_\beta = \frac{k_{r\beta}}{\mu_\beta} \rho_\beta \, \mathrm{PI}(\mathrm{P}_\beta - \mathrm{P}_{\mathrm{wb}}) \tag{2}$$

where q_β is mass rate (kg/s), $k_{r\beta}$ relative permeability, μ_β dynamic viscosity (Pa s), PI productivity index (m^3), P well block pressure (Pa), and P_{wb} flowing wellbore pressure (Pa). When the well is opened on multiple layers the flowing wellbore pressure needs to be estimated in front of each well block. A rigorous approach would require the solution of coupled wellbore-reservoir flow under transients conditions such as that implemented in T2Well (Pan and Oldenburg, 2104). TOUGH2 V2 implements the simplified approach due to Coats (1977) originally developed for hydrocarbon wells in which a gas and an oil phase of low mutual solubility were flowing.

The procedure gives a reasonable calculation of wellbore flowing pressure profile only in the presence of single-liquid conditions along the wellbore (Marcolini and Battistelli, 2012) as the gravitational contribution is predominant over friction and acceleration drops, which are completely neglected in the basic TOUGH2 V2 well model. Friction and acceleration drops can be significant in both two-

phase and single-gas flowing conditions, making the calculation of feed point rate unreliable. Moreover, if one well-block element has single-phase conditions, the density of the non-existing phase is missing, and the calculation of flowing density at wellbore node is erroneous.

Subroutine GCOR, where the calculation of flowing wellbore pressure is performed, has been modified by enforcing the calculation of density of the non-existing phase. The density is that of steam or water at saturation conditions for the current well-block temperature. This fix is available for all TOUGH2P EOS modules if the standard wellbore flow model is chosen. In addition, the capillary pressure contribution to the liquid phase pressure P_β in eq. 2 has been added and is used only if the IAPWS-IF97 correlations are chosen.

PetraSim now supports the specification of PI and well block pressure P_{wb} by layer. Once the well trajectory has been defined, PetraSim finds all the intercepted well-blocks and allows the user to input values for each of them.

During field-wide geothermal simulations make-up wells modeled using the deliverability approach are usually activated when the global steam rate declines below a prescribed target necessary to feed the power plant. This normally requires the user to check the simulation results, compute the discharged global steam rate, and find the time at which it is insufficient to match the given target rate value. Then the simulation is repeated up to the time identified above and a restart is performed that activates a new make-up well. A field wide geothermal simulation is then composed by a series of subsequent runs corresponding to the activation of make-up wells. The option to assign a specific activation time for each well on deliverability has been added. This makes it possible to perform the complete production forecast simulation in one run, using approximate activation times of make-up wells to be subsequently adjusted to match the steam rate target. When the final activation times have been defined, the results are obtained in a single run, rather than with a series of different simulation segments corresponding to the activation of make-up wells.

2.4 Miscellaneous modifications

Other miscellaneous modifications include:

- Optional output of mass and heat balance results computed at each time step. This is useful to check the approach to steady-state conditions which are usually accepted as a proxy for the natural state of geothermal systems.
- An option to write the restart file (file SAVE) after a time step interval, not just at the previously planned end of the run.
- An option has been added to force TOUGH2P to perform at least one NR iteration. This is often useful for steady-state runs once the final solution is approached.
- An option to save geometrical grid parameters in the input file (keywords MESH and MINC) with a 20 column format rather than the standard 10 column format, with a drastic reduction of truncation errors. Errors can arise when using UTM coordinates rather than a local spatial reference system, as it is common when building 3D field wide models of geothermal fields.

3. EWASG EOS MODULE

The EWASG module was originally developed (Battistelli et al., 1997) to model geothermal systems with fluid mixtures composed by water, NaCl and one NCG, which in high temperature geothermal reservoirs is almost always represented by CO_2. The code version distributed in 1999 suffers a few main limitations: correlations derived from different sources with the potential risk of limited internal coherence; brine correlations not covering properly the entire P-T-X space of interest; NCG effects evaluated with an approach limited to low partial pressures (Battistelli, 2012). Efforts to overcome some of the above limitations are described here below, with regard to the modeling of saline hydrothermal systems.

3.1 Brine density and enthalpy

Brine density is evaluated in EWASG by first computing the saturated brine density with Haas (1976) correlations, and then adding the effect of pressure by evaluating the brine compressibility with a correlation due to Andersen et al. (1992). An additional model is now available based on correlations proposed by Batzle and Wang (1992) for the brines commonly encountered in sedimentary basins. Their correlation reproduces the brine density data reported by Zarembo and Fedorov (1975) up to 350°C and salinity of 240,000 ppm. The inclusion of more recent correlations proposed by Driesner (2007) for the entire PTX range of interest and already successfully employed within a home version of EWASG (Battistelli, 2012) have been planned for future PetraSim releases.

EWASG uses a correlation due to Michaelides (1981) to compute the enthalpy of brine at vapor saturated conditions which is then corrected for the effect of pressure. The correlation was obtained by regression of enthalpy data in the 100-300 °C range and up to about 30% NaCl content. To conveniently work on a wider temperature range, two additional models have been added to evaluate the enthalpy of vapor saturated brines. The first one is based on the interpolation on tabular data provided by Phillips et al. (1981) for the 25-300°C temperature range and up to 250,000 ppm NaCl. Linear extrapolations are performed outside the above ranges. The second model is that due to Lorenz et al. (2000) already implemented in the ECO2N EOS module (Pruess, 2005). The correlation was obtained by regressing vapor saturated brine enthalpy data given by Pitzer et al. (1979) in the 25-300°C temperature range. The inclusion of more recent correlations proposed by Driesner (2007) for the entire PTX range of interest and already successfully employed within a home version of EWASG (Battistelli, 2012) have been planned for future PetraSim releases.

As shown by Garcìa (2001), the content of dissolved NCG affects the aqueous phase density. Battistelli et al. (2016) showed that the effect can be either an increment or a reduction of brine density depending on the type of NCG and P&T conditions, with dissolved NCG contributing to the development in deep sedimentary formations of convection fluxes driven by density differences. The Garcìa (2001) approach for the H_2O-CO_2 mixture has been extended to H_2O-NaCl-NCG ternary mixtures and can be optionally activated. The

molar volume of dissolved CO_2 and CH_4 is computed using a regression on experimental data by Hnědkovský et al. (1996) obtained from 25 to 350°C at 350 bar. That of N_2 and H_2 is evaluated using a regression on values computed using SUPCRT92 (Johnson et al., 1992) at 300 bar and from 0 to 300°C.

The dissolved NCG affects also the brine enthalpy. The existing approach is based on the calculation of NCG enthalpy in the gas phase and on the addition of the NCG heat of solution in the aqueous phase. The latter was computed by using the van 't Hoff equation as shown by Himmelblau (1959) by deriving the logarithm of Henry's constant with respect to temperature (Battistelli et al., 1997). This approach is acceptable for low partial pressures of the NCG, at which its enthalpy in the gas phase can be reliably evaluated with an ideal gas approach. When the NCG partial pressure becomes high, the NCG gas enthalpy is computed accordingly and the pressure effect is transmitted to the enthalpy of dissolved NCG as the heat of solution is computed neglecting the pressure. Koshel et al. (2006) showed that the enthalpy of NCG dissolved in the aqueous phase is almost constant with respect to pressure, indicating that the effect of pressure on the heat of solution is almost compensating that on gaseous NCG enthalpy. Thus, in addition of the previous approach a new one can be optionally chosen to calculate the enthalpy of dissolved NCG as a function of temperature only. This option can be used when CO_2 is chosen as NCG to be simulated, as only the enthalpy of gaseous CO_2 is computed as function of both temperature and pressure.

3.2 Halite properties

EWASG can simulate the precipitation/dissolution of solid NaCl (halite), which may occur because of persistent boiling of a brine solution. New correlations for halite properties are now used in EWASG if the IAPWS-IF97 correlations are chosen. Old and new correlations are as follows:

- Halite solubility in the liquid phase (XEQ): the Potter's equation quoted by Chou (1987) is substituted by the Driesner and Heinrich (2007) correlation.

- Halite solubility in the vapor phase: the old constant NaCl concentration threshold (1.E-12 kg/kg) is now substituted by solubility values computed as function of temperature. First the NaCl solubility in the vapor phase in equilibrium with halite saturated brines (XEQG) is computed according to Palliser and McKibbin (1998). Then the mass fraction in the vapor phase (XSG) is computed assuming a linear dependence with respect to the mass fraction in the liquid phase (XS) as follows:.

$$XSG = XS\frac{XEQG}{XEQ} \tag{3}$$

  This approximate relationship was included in order to improve the modeling of saline systems when persistent boiling progressively concentrates the NaCl in the brine promoting halite precipitation. The former approach simulated the precipitation of halite even for initial concentrations in order of few ppm of NaCl in the liquid phase, with strong lowering of the vapor pressure of steam-water mixtures. In addition, the G+S ←→G+S+L phase transition was occasionally affected by numerical instabilities, which are now alleviated by the more realistic treatment, even though still approximate, of NaCl transport in the gas phase.

- Halite enthalpy: it was computed by integrating the specific heat given by Silvester and Pitzer (1976). The resulting correlation was affected by an erroneous choice of the reference conditions of halite enthalpy which must be congruent with the enthalpy of NaCl brine (Battistelli, 2012), which has been already fixed within PetraSim. A new correlation is now available derived from that given by Driesner (2007) which accounts for the effects of both temperature and pressure as described in Battistelli (2012).
- Halite density: it was computed as function of temperature and pressure using a correlation due to Silvester and Pitzer (1976). A new correlation derived from that proposed by Driesner (2007) can now be optionally used (Battistelli, 2012).

3.3 Permeability change due to halite precipitation

EWASG simulates the effects of halite precipitation on rock permeability following the models developed by Verma and Pruess (1988) for the precipitation of silica in porous and fractured media. In particular the models implemented were: i) constant pore diameter or constant fracture aperture; ii) series model for planar parallel fractures; iii) series model for parallel tubes. Three new options are now available: iv) Model 1 by Weir and White (1995); v) Model 2 by Weir and White (1995); and vi) the generalized model with critical porosity suggested by Xu and Pruess (2004).

4. EOS2 MODULE

The EOS2 module was originally developed by O'Sullivan et al. (1985) to model geothermal systems with relevant amounts of CO_2, the most abundant NCG in high temperature geothermal reservoirs. The original code version uses thermodynamic equilibrium and thermo-physical correlations which loose accuracy at increasing CO_2 partial pressures. Efforts to overcome some of the above limitations are described here below, with special regard to the modeling of geothermal systems.

4.1 CO_2 density

In EOS2 the density of gaseous CO_2 is computed using the Plank-Kuprianoff correlation which was initially employed by Sutton (1976). That equation loses accuracy at high pressures and low temperatures and can even provide negative densities when pressure and temperature conditions approaches the critical point of CO_2. A new option allows the calculation of pure CO_2 density using the Peng

and Robinson (1976) cubic EOS which gives reasonable accurate density values from 0 to 350°C and up to 500 bar partial CO_2 pressure. Below the critical temperature of CO_2, the density of both gaseous or liquid CO_2 can be computed, eliminating the problems present when using the Plank-Kuprianoff original equation. Under these conditions a test for the choice of the proper root of the cubic equation of state when more than one root is present has been added following Nghiem and Li (1989). It must be reminded that 3-phase conditions, with both liquid and gaseous CO_2 cannot be handled by EOS2.

4.2 CO_2 solubility and heat of solution

The solubility of CO_2 in water was computed by O'Sullivan et al. (1985) using the Henry's law with a correlation of Henry's constant providing reliable values only within the 40-330°C range. For this reason, the TOUGH2 V2 release (Pruess et al., 1999) implemented into the EOS2 module the Henry's constant regression over experimental data by Cramer (1982) from 0 to 300°C and by D'Amore and Truesdell (1988) from 300° to 370°C employed by EWASG (Battistelli et al., 1997), which is more accurate in the 0-350°C range. In order to improve the solubility calculations at high CO_2 partial pressures the Poynting correction has been applied. The condition for thermodynamic equilibrium of a two-phase H_2O-NCG mixture requires the equality of components fugacity in both phases. Using the Henry's law and the Poynting correction for the aqueous phase, the condition for the equality of NCG fugacities can be written as follows (Li and Nghiem, 1986):

$$\phi_G^{NCG} y_G^{NCG} P = K_h^{NCG}(T)\, y_L^{NCG} \exp\left(\frac{\int_{P_0}^{P} v^{NCG}(T,P)dP}{R\,T_K}\right) \tag{3}$$

where ϕ, y, P, K_h, R, T, and v are fugacity coefficient, molar fraction, pressure (Pa), Henry's constant (Pa^{-1}), universal gas constant, temperature (K), and molar volume (cc/mol) of dissolved NCG in the aqueous phase, respectively. Assuming an average value of the NCG molar volume is used between the saturation pressure of water and that of the two-phase mixture, and assuming a unit gas fugacity coefficient for CO_2, eq. 3 becomes:

$$y_G^{CO2} P = K_h^{CO2}(T)\, y_L^{CO2} \exp\left(\frac{v^{CO2}(T)\times(P - P_{sat}(T))}{R\,T_K}\right) \tag{4}$$

The molar volume of dissolved CO_2 has been used as a regression parameter in order to reproduce the CO_2 solubility at 300 bar given by Duan and Sun (2003) from 10 to 250°C and by Spycher and Pruess (2010) from 250 to 300°C.

The CO_2 heat of solution is computed in the original EOS2 module using a regression on data published by Ellis and Goulding (1963) which were obtained by using the van 't Hoff equation and by deriving the Henry's constant determined with experimental CO_2 solubility data. As an optional choice, now the heat of solution may be computed using the same approach but deriving the Henry's constant employed in the EWASG EOS module. In addition, the enthalpy of CO_2 dissolved in the aqueous phase may be computed as already described above for the EWASG EOS module.

4.3 Improving phase transition convergence

Phase transitions occurring during TOUGH2 numerical simulations are occasionally affected by numerical instabilities which may be related to the high non-linear processes occurring across phase transitions, the approximate evaluation of primary variables to be switched, as well as to the difficulties to interpolate the phase parameters at the interface between grid blocks. The latter problem has been studied by O'Sullivan et al. (2013; 2014) for the EOS modules commonly employed for geothermal reservoir simulation, including EOS1, EOS2, EOS3 and EWASG. In order to obtain a stable interpolation of phase density across a phase transition, they implemented the calculation of the density of non-existing phase. The same approach is now optionally available in EOS2 supported by PetraSim. In addition, the same option performs also the calculation of enthalpy and viscosity of the non-existing phases, in a way similar to that implemented into iTOUGH2 (Finsterle, 2016).

4.4 Optional initialization of primary variables

The primary variables used by EOS2 are pressure, temperature and partial pressure of CO_2 (P-T-PCO2) for single phase conditions, and pressure, gas phase saturation and partial pressure of CO_2 (P-SG-PCO2) for two-phase conditions. Thus, PCO2 is always used to define the amount of CO_2 present in the mixture. While this can be useful in many applications, in others it can make the input of initial conditions rather complicate. An example is the case where an aquifer has variable temperature conditions but a constant composition. To obtain a constant mass fraction of dissolved CO_2, the input partial pressure should change as function of temperature. In this case the direct input of CO_2 mass fraction would be more useful. Thus, two new options to initialize single-phase liquid and two-phase conditions have been included, as shown in Table 1.

PHASE CONDITION	PRIMARY VARIABLES
SINGLE-PHASE GAS	P, T, PCO2.
SINGLE-PHASE LIQUID	P, T, PCO2 or **P, T, -XCO2L.**
TWO-PHASE	P, SG, PCO2 or **T, SG, PCO2.**

Table 1: Primary variables used by EOS2. Two new options (in bold) are added to the original choice available. XCO2L is the mass fraction of CO_2 dissolved in the liquid phase.

5. MODIFICATIONS OF PETRASIM INTERFACE

The PetraSim interface has been extended to support the above options. In general, these appear as additional choices on the dialogs related to the specific EOS being used. Other changes in PetraSim 2017 include:

- The comma-separated values output files have additional output data, for example, the time-dependent source/sink data now includes the flow fraction of NaCl and NCG for EWASG.
- Export of both 3D and well plot results now includes all data, not just the output parameter being plotted. This gives the user all the data needed to plot multiple parameters without making multiple plots in PetraSim.
- The ability to enable or disable wells in the model. The user can now specify all the wells that will be used in the model and enable only the specific wells that will be used for a particular simulation.
- Printout of the relative permeability and capillary pressure values as a function of liquid saturation for all rock domains.

6. NUMERICAL SIMULATIONS

A couple of numerical simulations performed using TOUGH2P V2.0 – EWASG are discussed here below to compare the results obtained with some of the new options described above with those of former TOUGH2 V2 and EWASG released with PetraSim.

6.1 EWASG: RHBC sample problem (#1)

A first simple comparison between the old TOUGH2-EWASG supported by PetraSim and the one implementing the new options described above is presented by using a slightly modified version of the EWASG sample problem RHBC described in detail in the TOUGH2 V2 user's guide (Pruess et al., 1999). The version here used is that described by Thunderhead Eng. in the PetraSim support documentation: Michaelides (1981) is used for the brine enthalpy and Hass (1976) and Anderson et al. (1992) for the brine density, with the old IFC (1967) correlations for pure water. The initial time step has been changed from 10000 s to 100 s, the time step is doubled when convergence is achieved within 3 iterations instead of 4, and the simulation is extended from 2.E6 s (23.1 days) to 5.184E6 s (60 days). A constant rate production of 65 kg/s is extracted from a 1D radial reservoir of 500 m thickness, and 1000 m radial extension, initially in two-phase conditions with liquid phase saturation SL=0.55, which is higher than the irreducible saturation of 0.30 used for the Corey (1954) liquid phase relative permeability, pressure of 60 bara, temperature of 275.55°C and salt mass fraction of 0.30. The initial partial pressure of CO_2 is equal to 14.788 bar.

Three runs have been made using A) old options only; B) IAPWS-IF97 correlations for pure water, which also enforce NaCl solubility in halite saturated steam as function of temperature, and new options to evaluate the enthalpy of dissolved NCG, and the enthalpy and density of halite; C) IAPWS-IF97 correlations, plus Lorenz et al. (2000) for brine enthalpy and Batzle and Wang (1992) for brine density. The partial pressure of CO_2 and some phase properties at initial conditions for the 3 runs are listed in Table 2, together with the number of time steps and NR iterations needed to complete the simulation. Run B&C have a slightly higher PCO_2 because the water vapor pressure is computed using IAPWS-IF97. As a consequence CO_2 mass fraction in the liquid and gas phase is slightly higher. The brine density is slightly lower for run B with respect to run A because of combined effect of IAPWS-IF97 and dissolved CO_2. A remarkable reduction is observed for run C which uses the Batzle and Wang (1992) correlation for brine density. The viscosity of both brine and gas phase changes due to the IAPWS-IF97 used for runs B & C. The major change for the enthalpy is for run C as the brine enthalpy is computed according to Lorenz et al. (2000). The mass fraction of NaCl in the gas phase increases when instead of a constant solubility value in the halite saturated steam, the solubility is computed as function of temperature according to Palliser and McKibbin (1998) and eq. 3. The effects of the new options on the simulation speed are limited, with a slight increment of time steps and NR iterations from run A to B, and substantially similar values from run A to C. Thus, for this simple problem the new options do not adversely affect the simulation speed.

Run #	PCO_2 (bar)	XCO2L	XCO2G	ρ_L (kg/m^3)	ρ_G (kg/m^3)	μ_L (Pa s)	μ_G (Pa s)	h_L (kJ/kg)	h_G (kJ/kg)	XNaClG	Time steps	NR iterations
A	14.788	6.7160E-4	0.40316	1040.8	35.578	2.3570E-4	2.1531E-5	876.90	1813.4	8.2758E-13	96	374
B	14.810	6.7264E-4	0.40398	1040.4	35.560	2.3614E-4	2.1470E-5	876.80	1812.1	6.0444E-07	100	390
C	14.810	6.7264E-4	0.40398	990.96	35.502	2.3614E-4	2.1470E-5	810.84	1812.1	6.0444E-07	97	376

Table 2: EWASG sample problem #1. Parameters at initial conditions, total time steps and NR iterations for the 3 runs.

Figure 1(left) shows pressure (P), CO_2 partial pressure (PCO2), gas saturation (SG), solid saturation (SS) and salt mass fraction in the brine (XNaCl_L) computed at two times of 0.5E6 s and 2.0E6 s and plotted as function of the similarity variable R^2/t. Because of radial symmetry, homogeneous petrophysical properties, uniform initial conditions and constant mass withdrawal, the similarity solution applies according to O'Sullivan (1981). Figure 1 shows that the results respect the similarity solution, as already shown in Pruess et al. (1999) indicating the accuracy of numerical solution. The pressure drawdown produces the evaporation of the brine which eventually disappears close to the production well. NaCl is concentrated in the boiling brine inducing halite precipitation with porosity and permeability reduction. Figure 1 (right) shows the comparison of similarity results obtained at 2.E6 s for the three runs. Results of run B & C basically follows those of run A, but the pressure (P) and the gas phase saturation (SG) close to the wellbore. Figure 2 (left) shows the production enthalpy (H) and the well-block pressure vs time for the three runs, while the CO_2 and NaCl mass fraction in produced fluid are shown in Figure 2 (right), the major difference being the higher NaCl concentration due to its higher solubility in the gas phase.

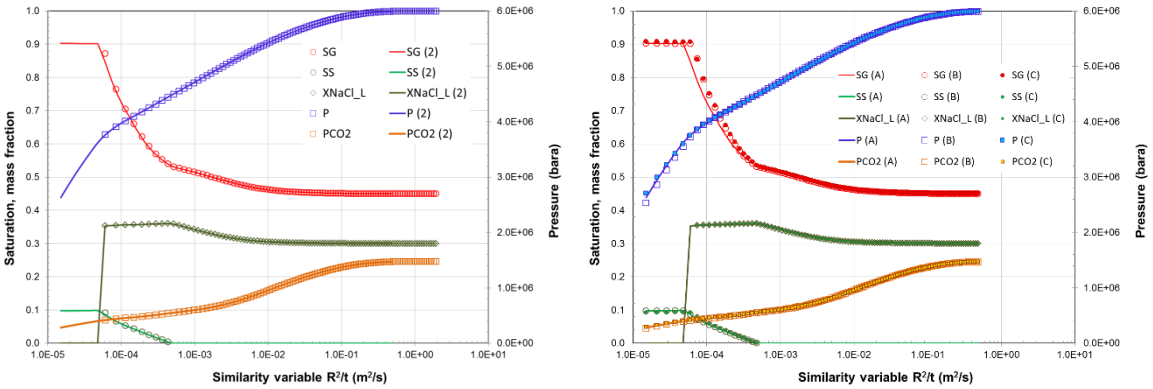

Figure 1: EWASG sample problem #1. Left: run A similarity results at time 0.5E6 (symbol) and 2.0E6 s (line). Right: similarity results at time 2.0E6 s for runs A (line), B (empty symbols) and C (bold symbols).

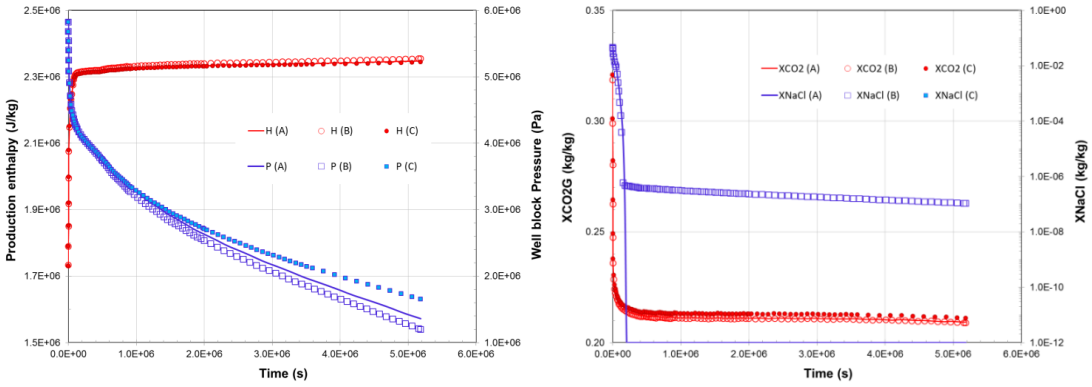

Figure 2: EWASG sample problem #1. Left: production enthalpy and well block pressure vs time. Right: CO_2 and NaCl (log scale) mass fraction in produced fluid. Runs A (line), B (empty symbols) and C (bold symbols).

6.2 EWASG: salt water injection into a depleted vapor dominated reservoir (sample problem #2)

A further comparison between the old TOUGH2-EWASG supported by PetraSim and the one implementing the new options is presented using a 2D radial model employed by Calore and Battistelli (2003) to simulate the injection of salt water into a depleted high temperature vapor dominated reservoir. The reservoir is modeled as a 2-D radial, homogeneous and isotropic porous medium with a radius and height of 2 km, porosity 0.01 and permeability 10E-15 m^2 (Figure 3).

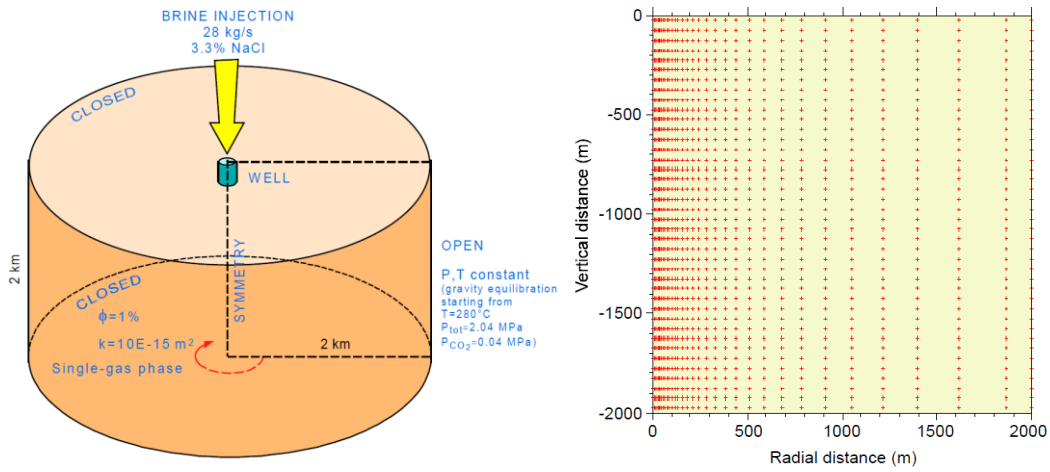

Figure 3: EWASG sample problem #2. Left: 2-D radial model with location of injection well. Right: location of element nodes. After Calore and Battistelli, 2003).

Initial conditions at the top were: total pressure 2.04 MPa, temperature 280°C, and CO_2 partial pressure 0.04 MPa, with gravity equilibrium in the rest of the system. Corey's relative permeability functions were used, with irreducible liquid saturation SLR=0.80 and irreducible gas saturation SGR=0.05. Capillary pressure effects were introduced using van Genuchten's model (van Genuchten, 1980), with the following parameters: m=0.4438, SLR=0.08, 1/P0=5.792E-7 Pa^{-1}, Pmax=5.E7 Pa and SLS=1. Molecular diffusion fluxes were considered by computing the effect of phase tortuosity using the Millington and Quirk (1961) model. Diffusion coefficients were 1E-5 m^2/s and 1E-10 m^2/s for mass components in the gas and liquid phases, respectively. The changes in porosity caused by salt precipitation and the consequent reduction in permeability were modelled by the "tube-in-series" model (Verma and Pruess, 1988), with a critical porosity of 80%. This high value of critical porosity causes mass flows to drop to zero for a reduction in pore volume of 20%. The model is discretized in 40 layers of 50 m thickness, and 51 columns with a logarithmic increment of elements width. The location of grid nodes is shown in Figure 3(right). The injection well is located on the axis of the 2-D radial model and is completed on the top 200 m. Constant brine is injected for 30 years at a total rate of 28 kg/s with NaCl fraction of 3.3%.

Four runs are described below: A) uses old EWASG options; B) as A, but using the IAPWS-IF97 correlations, Lorenz et al. (2000) and Batzle and Wang (1992); C) as B, but assigning an entry gas pressure of about 2 bar at 280°C (with SLS=1.01) and the scaling of capillary pressure as function of temperature, assuming as the reference values those already used at 280°C; D) as C, but with the linear extrapolation of capillary pressure for liquid saturations lower than SL=0.18. The choice to maintain as reference curve the original at 280°C , which increases the capillary pressure at lower temperature to quite high values, was made for an easier comparison with runs A & B. The different capillary pressure curves used are plotted in Figure 4 using the values now written by EWASG on the output file for each rock domain.

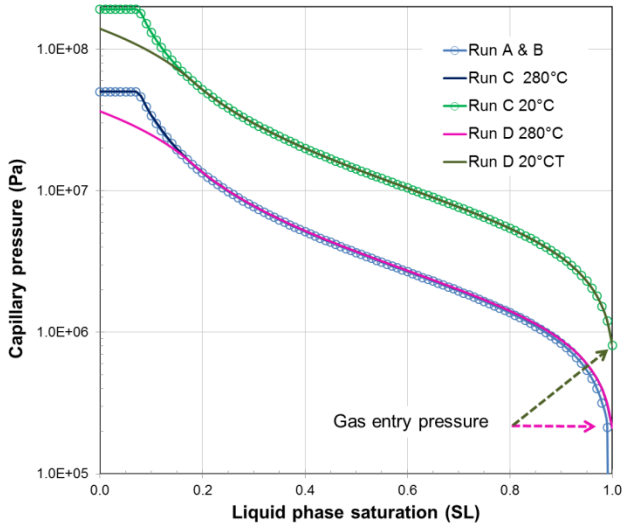

Figure 4: EWASG sample problem #2: brine injection in a vapor dominated reservoir. Run A & B: original VG curve at 280°C; run C:VG with gas entry pressure, and scaling; run D: as per run C) plus linear extrapolation below SL=0.18. In addition to the original capillary pressure at 280°C, those computed at T20°C are also plotted.

Run #	Time steps	NR iterations	Time step fraction	NR iterations fraction
A	10144	66379	1.000	1.000
B	8945	57942	0.882	0.873
C	5797	36828	0.571	0.555
D	5399	35194	0.532	0.530

Table 3: EWASG sample problem #2. Total time steps and cumulative NR iterations of converged time steps for the 4 runs. Fraction of time steps and NR iterations with respect to run A.

Table 3 lists the time steps and cumulative NR iterations for converged time steps necessary to complete the runs. From Run A to B the reduction of time steps and NR iterations is in the order of 12 –13%. This should be mainly due to the different handling of NaCl solubility in the gas phase which affects the G←→G+L phase transition. Time steps and NR iterations are reduced by about 43 –45% for run C thanks to the inclusion of gas entry pressure and capillary pressure scaling. As the capillary pressure is drastically changed because of temperature scaling, this reduction is also due to the different shape of liquid plume and related different number of encountered phase transitions. The introduction of linear extrapolation of capillary pressure for run C produced a slightly higher reduction of time steps and NR iterations in the order of 47%.

A first comparison of four runs is made by looking at the mass of liquid phase vs time contained in the modeled domain shown in Figure 5. The same figure also shows the fraction of injected brine which is still liquid as function of time. These are important parameters as indicate how much brine has vaporized supplying steam for production wells. In our model the production wells are not explicitly modeled, but are assumed to be responsible for the constant pressure conditions maintained at the lateral model boundary. Both parameters plotted in Figure 5 are substantially identical for the 4 runs during the first 8 years when the non-vaporized injected brine amounts to about 15.5%. The differences become appreciable after about 21 years: after 30 years the non-vaporized brine fraction is about 14.5% for run A & B and about 13.7% for runs C & D.

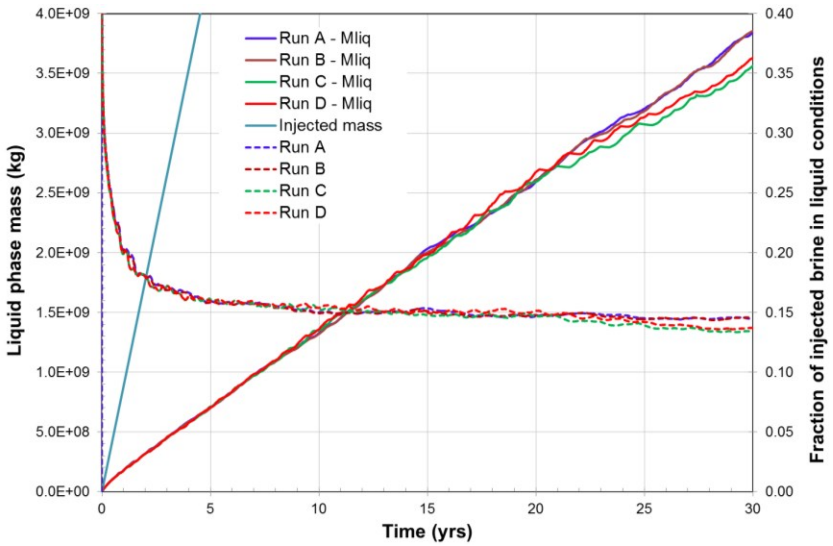

Figure 5: EWASG sample problem #2. Liquid phase mass and fraction of injected brine in liquid conditions vs time for runs A, B, C and D. The cumulative injected mass is plotted for comparison.

A further comparison is made looking at the mass of solid salt and gas phases in Figure 6. While the gas phase mass evolution is substantially similar for the 4 runs, the salt mass fraction for runs C & D basically departs from that of runs A & B after 5 years brine injection remaining always lower till the end of the simulation. The gas phase mass increases during the first year as the vaporized steam pressurizes the model domain with limited outflow through the lateral boundary. After 1 year the gas phase mass steadily declines but remaining at values higher than the initially stored mass. The differences among the 4 runs are minor.

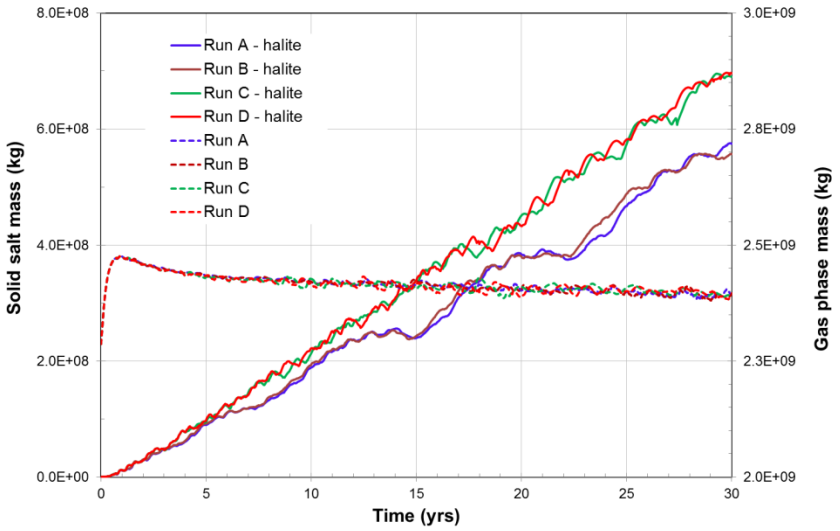

Figure 6: EWASG sample problem #2. Liquid phase mass and fraction of injected brine in liquid conditions vs time for runs A, B, C and D.

Previous plots have highlighted that runs A & B are similar as well as runs and C & D. Thus, the analysis of spatial distribution of main reservoir properties after 30 years of brine injection will be limited to the comparison of runs A and D. Figures 7 and 8 show the spatial distribution of temperature, pressure, gas and solid phases saturation for runs A and D, respectively. The distribution of gas phase saturation for run A is essentially congruent with the distribution of liquid plume shown previously by Calore and Battistelli (2003). As already discussed by them, the plume of liquid brine is at injection temperature (about 30°C) just around the injection wells and gradually is heated to approach the reservoir temperature. Two-phase conditions are delimited by the halite precipitation zone in which solid saturations exceeding 0.2 are found because of brine evaporation and concentration of NaCl in the residual brine. Thus, the following fronts are traveling from the injection well: liquid brine at injection T, heated liquid brine, two-phase conditions, and the zone of halite precipitation and complete vaporization of liquid brine. The halite zone is characterized by the dissolution and precipitation of solid salt at its inner and outer boundaries, respectively.

As far as the shape of liquid plume is concerned, at the beginning of injection the plume preferentially expands in the radial direction due to the high injection pressure gradient, which declines quickly with radial distance with plume expansion. The radial plume expansion almost stabilizes when the increasing downward gravity driven flow starts to balance the injected rate. From this point on, the plume preferentially expands downwards under the influence of gravity. Further lateral expansion is related to the permeability reduction at the front of down flowing brine and to the effect of capillary pressure. The pressure distribution shows the gradient that drives steam towards the lateral constant pressure boundary. High pressures are experienced only at the injection well (125-137 bara).

While the liquid brine reaches the bottom of the model at -3000 m for run A (Figure 7), it reaches of only -2300 m for run D (Figure 8), with a larger expansion on the radial direction at the plume bottom. The inclusion of gas entry pressure in the VG capillary pressure curve essentially improves the disappearance of liquid phase but has a limited impact on brine flow as at saturations far from unity the capillary pressure is basically the same, as shown in Figure 4. The liquid plume shape for runs C (not shown) and D is quite similar indicating that the linear extrapolation of capillary pressure slightly improves the numerical performances with limited effects on flow processes. Thus, the main modification responsible for the quite different liquid plume shape between runs A and D is the inclusion of capillary pressure scaling with temperature, which consistently increases the capillary pressure at low temperature (see Figure 4).

6. CONCLUSIONS

A new release of PetraSim-TOUGH2P V2.0 including updated fluid thermodynamics calculations and improvements related to flow processes and the treatment of production wells has been described. While some of the improvements are applicable to all the TOUGH2P EOS modules supported by PetraSim 2017, the primary focus is the EOS modules customarily used for the modelling of geothermal reservoirs: EOS1 for pure water, EOS2 for water-CO_2 mixtures, and EWASG for ternary H_2O-CO_2-NaCl mixtures. A couple of sample problems simulated using TOUGH2P V2.0 – EWASG have been presented and the effect of some of the new available options have been discussed in detail.

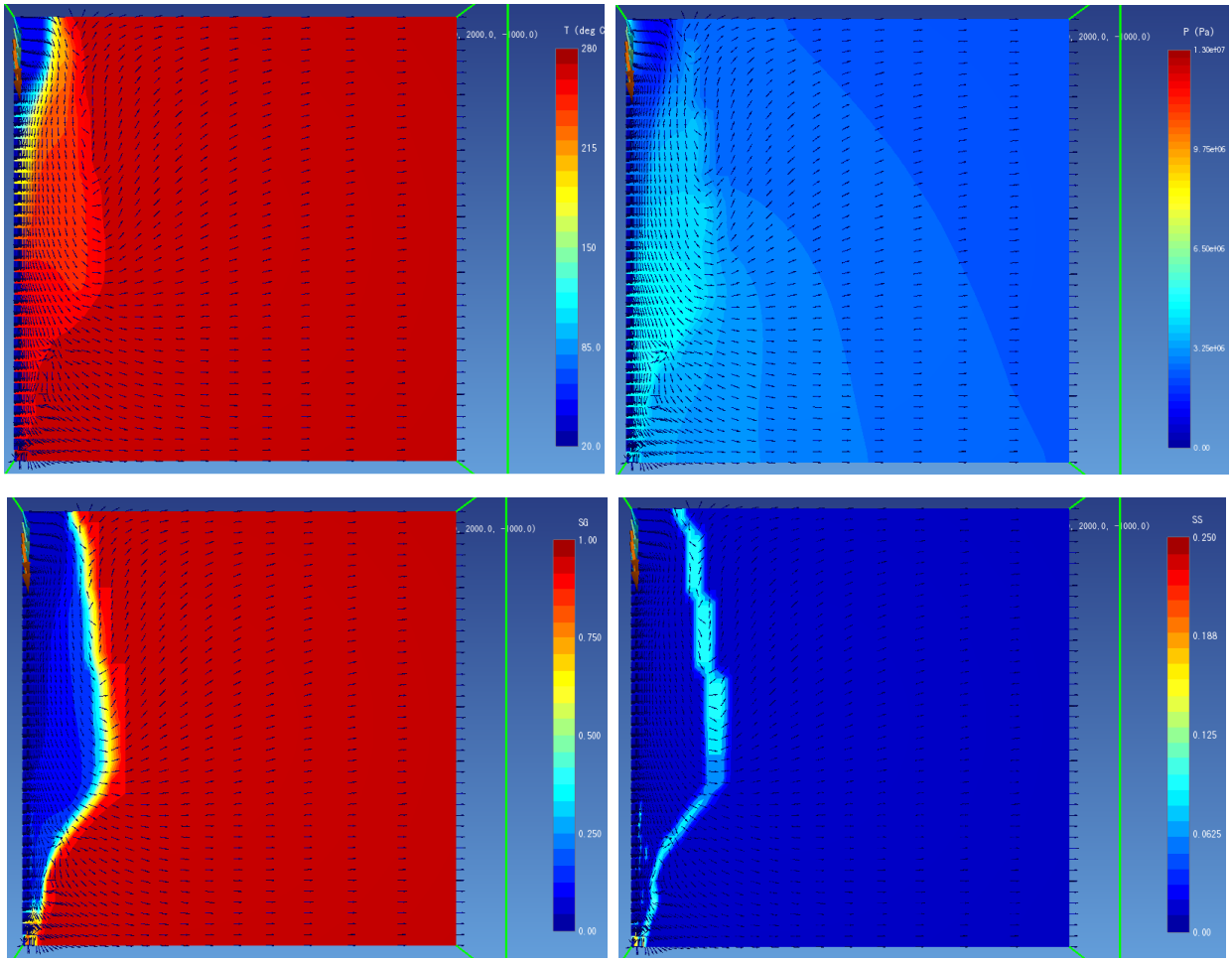

Figure 7: EWASG sample problem #2. Spatial distribution of temperature, pressure, gas and solid phases saturation after 30 years of brine injection for run A.

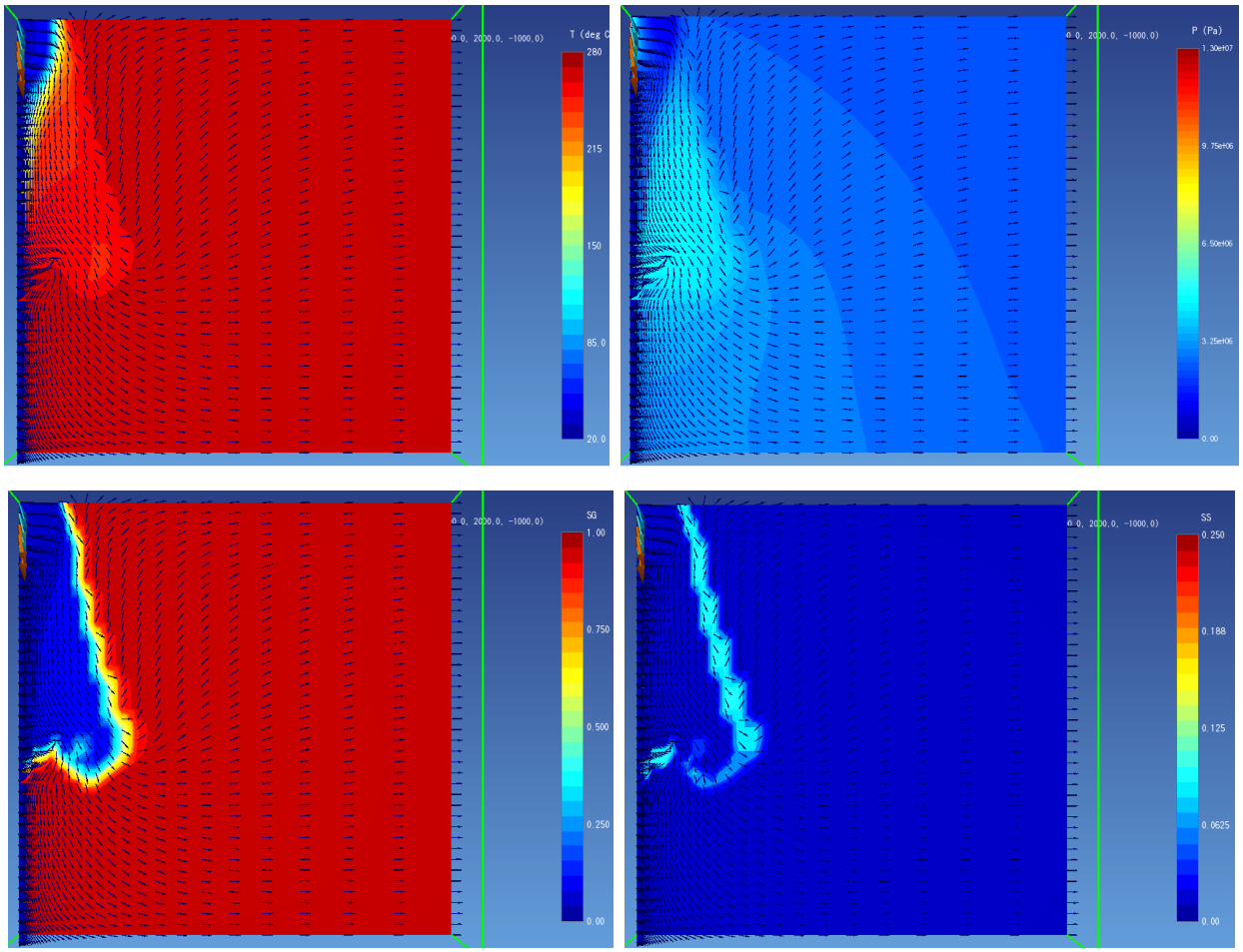

Figure 8: EWASG sample problem #2. Spatial distribution of temperature, pressure, gas and solid phases saturation after 30 years of brine injection for run D.

REFERENCES

Andersen, G., Probst, A., Murray L., Butler S.: An accurate PVT model for geothermal fluids as represented by H_2O-NaCl-CO_2 mixtures, *Proceedings* 17th Workshop on Geothermal Reservoir Engineering, Stanford University, Stanford, CA (1992).

Battistelli, A., Calore, C., Pruess, K.: The simulator TOUGH2/EWASG for modelling geothermal reservoirs with brines and a non-condensible gas, *Geothermics*, **26**, (1997), 437-464.

Battistelli, A.: Improving the treatment of saline brines in EWASG for the simulation of hydrothermal systems, *Proceedings*, TOUGH Symposium 2012, Lawrence Berkeley National Laboratory, Berkeley, CA (2012).

Battistelli, A., Berry, P., Bonduà, S., Bortolotti, V., Consonni, A., Cormio, C., Geloni, C., Vasini, E.M.: Thermodynamics related processes during the migration of acid gases and methane in deep sedimentary formations, *Greenhouse Gas Science and Technol.*, doi:10.1002/ghg.1614, (2016).

Batzle, M., and Wang, Z.: Seismic properties of pore fluids, *Geophysics*, **57**, (1992), 1396–1408.

Brooks, R.H., and Corey, A.T.: Properties of Porous Media Affecting Fluid Flow, *J. Irrig. Drain. Div.*, 6, 61,(1966).

Calore, C., and Battistelli, A.: Application of TOUGH2/EWASG to the modelling of saltwater injection into a depleted geothermal reservoir: preliminary results. *Proceedings TOUGH Symposium 2003*, Lawrence Berkeley National Laboratory, Berkeley, CA, (2003).

Coats, K.H.: Geothermal reservoir modelling, *Paper SPE 6892*, (1977).

Chou, I. M.: Phase relations in the system NaCl-KCl-H_2O. III: Solubilities of halite in vapor-saturated liquids above 445°C and redetermination of phase equilibrium properties in the system NaCl-H_2O, *Geochimica et Cosmochimica Acta*, **51**, (1987), 1965-1975.

Corey, A.T.: The Interrelation Between Gas and Oil Relative Permeabilities, *Producers Monthly*, Nov. 1954 (1954), 38-41.

Cramer, S. D.: The solubility of methane, carbon dioxide and oxygen in brines from 0° to 300°C, *US Bureau of Mines*, Report No. 8706, (1982)..

Croucher, A.E., and O'Sullivan, M.J.: Application of the computer code TOUGH2 to the simulation of supercritical conditions in geothermal systems, *Geothermics*, **37**, (2008), 622–634.

D'Amore, F., and Truesdell, A.H.: A review of solubilities and equilibrium constants for gaseous species of geothermal interest, *Science Geological Bulletin*, **41**, (1988), 309-332.

Driesner, T., and Heinrich, C.H.: The system H_2O–NaCl. Part I: Correlation formulae for phase relations in temperature–pressure–composition space from 0 to 1000°C, 0 to 5000 bar, and 0 to 1 XNaCl, *Geochimica et Cosmochimica Acta*, **71**, (2007),4880–4901.

Driesner ,T.: The system H_2O–NaCl. Part I: Part II: Correlations for molar volume, enthalpy, and isobaric heat capacity from 0 to 1000°C, 1 to 5000 bar, and 0 to 1 XNaCl, *Geochimica et Cosmochimica Acta*, **71**, (2007),4902–4919.

Duan, Z.H., and Sun, R.: An improved model calculating CO_2 solubility in pure water and aqueous NaCl solutions from 273 to 533 K and from 0 to 2000 bar, *Chem. Geol.*, **193**, (2003), 257-271.

Ellis, A.J., and Golding, R.M.: The solubility of carbon dioxide above 100°C in water and in sodium chloride solutions, *American Journal of Science*, **261**, (1963), 47-60.

Finsterle, S.: Personal communication, (2016).

García, J.E.:. Density of Aqueous Solutions of CO_2, Lawrence Berkeley National Laboratory, Report LBNL-49023, Berkeley, CA, (2001).

Johnson, J.W., Oelkers, E.H., and Helgeson, H.C.: SUPCRT92: A software package for calculating the standard molal thermodynamic properties of minerals, gases, aqueous species, and reactions from 1 to 5000 bars and 0 to 1000 degrees C, *Computers and Geosciences*, **18**, (1992), 899–948.

Himmelblau, D.M.:. Partial Molal Heats and Entropies of Solution for Gases Dissolved in Water from the Freezing to the Near Critical Point, *J. of Phys. Chem.*, **63**, (1959), 1803–1808.

Hnědkovský ,L., Wood, R.H., and Majer, V.: Volumes of aqueous solutions of CH_4, CO_2, H_2S, and NH_3 at temperatures from 298.15 K to 705 K and pressures to 35 MPa, *J. Chem. Thermodynamics*, **28**, (1996), 125–142.

IAPWS: Release on the IAPWS Formulation 2008 for the Viscosity of Ordinary Water Substance, Berlin, Germany, (2008).

IAPWS: Revised Release on the IAPWS Industrial Formulation 1997 for the Thermodynamic Properties of Water and Steam, IAPWS Release, Switzerland, (2007).

IFC: A Formulation of the Thermodynamic Properties of Ordinary Water Substance, IFC Secretariat, Düsseldorf, Germany, (1967).

Koschel, D., Coxam ,J.-Y., Rodier, L., and Majer, V.: Enthalpy and solubility data of CO_2 in water and NaCl(aq) at conditions of interest for geological sequestration, *Fluid Phase Equilibria*, **247**, (2006), 107–120.

Leverett, M.C.: Capillary Behavior in Porous Solids, *Trans. Soc. Pet. Eng. AIME*, **142**, (1941), 152-169.

Li, Y.-K., and Nghiem, L.X.: Phase equilibria of oil, gas and water/brine mixtures from a cubic equation of state and Henry's law, *Canadian Journal of Chemical Engineering*, **64**, (1986), 486 – 496.

Lorenz, S., Maric, D., and Rirschl, C.: Eine analytische Funktion zur Bestimmung der Enthalpie wässriger NaCl-Lösungen, *Report ISTec - A – 447*, (2000)

Marcolini, M., and Battistelli, A.: Modeling of wellbore flow within geothermal reservoir simulations at field scale. *Proceedings*, TOUGH Symposium 2012, Lawrence Berkeley National Laboratory, Berkeley, CA (2012).

Michaelides, E.E.: Thermodynamic properties of geothermal fluids, *Geothermal Resources Council Transactions*, **5**, (1981), 361-364.

Nghiem, L.X., and Li, Y.K.: Phase-equilibrium calculations for reservoir engineering and compositional simulation. In: *Second International Forum on Reservoir Simulation*, Alpbach, Austria, (1989).

O'Sullivan, M.J.: A Similarity Method for Geothermal Well Test Analysis, *Water Resour. Res.*, **17**, 2, (1981), 390 – 398.

O'Sullivan, M.J., Bodvarsson, G.S., Pruess, K., and Blakeley, M.R.: Fluid and heat flow in gas-rich geothermal reservoirs, *Society of Petroleum Engineers Journal*, **25**, (1985), 215-226.

O'Sullivan, J., Croucher, A., Yeh, A., and O'Sullivan, M.:. Improved convergence for air-water and CO_2-water TOUGH2 simulations, *Proceedings* 35th New Zealand Geoth. Work. , Rotorua, New Zealand, (2013).

O'Sullivan, J., Croucher, A., Yeh, A., and O'Sullivan, M.:. Further improvements in the convergence of TOUGH2 simulations. *Oñate E., Oliver J. and Huerta A. (Eds)*. 11th World Congress on Computational Mechanics (WCCM XI), (2014).

Palliser, C., and McKibbin, R.: A model for deep geothermal brines,I: T-p-X state-space description, *Transport in Porous Media*, **33**, (1998), 65-80.

Pan, L., and Oldenburg, C.M.: T2Well – An integrated wellbore-reservoir simulator, *Computer & Geosciences*, **65** (2014), 46-55.

Peng, D.-Y., and Robinson, D.B.: A New Two-Constant Equation of State, *Industrial & Engineering Chemistry Fundamentals*, **15**, (1976), 59 – 64.

Phillips, S. L., Igbene, A., Fair, J. A., Ozbek, H., and Tavana, M.: A technical databook for geothermal energy utilization, *Lawrence Berkeley Laboratory, Report LBL-12810*, Berkeley, CA, (1981).

Pitzer, K.S., Bradley, D.J., Rogers, P.S.Z., and Peiper, J.C.: Thermodynamics of High Temperature Brines, Lawrence Berkeley Laboratory, Report LBL-8973, Berkeley, CA (1979).

Pruess, K., Oldenburg, C.M., and Moridis, G.J.: TOUGH2 User's Guide, Version 2.0, *Lawrence Berkeley National Laboratory, Report LBNL-43134*, Berkeley, CA, (1999).

Pruess, K.: ECO2N : A TOUGH2 Fluid Property Module Mixtures of Water, NaCl and CO_2, *Lawrence Berkeley National Laboratory Report LBNL-57952*, Berkeley, CA (2005).

Pruess, K.: Personal communication, (2007).

Silvester, L.F., and Pitzer, K. S.: Thermodynamics of geothermal brines - I. Thermodynamic properties of vapor-saturated NaCl (aq) solutions from 0-300°C, *Lawrence Berkeley Laboratory, Report LBL-4456*, Berkeley, CA, (1976).

Spycher, N., and Pruess, K.: A Phase-Partitioning Model for CO_2–Brine Mixtures at Elevated Temperatures and Pressures: Application to CO_2-Enhanced Geothermal Systems, *Transport in Porous Media*, **82**, (2010), 173-196.

Sutton, F.M.: Pressure-temperatures curves for a two-phase mixture of water and carbon dioxide, *New Zealand Journal of Science*, **19**, (1976), 297-301.

van Genuchten, M. Th.: A closed-form equation for predicting the hydraulic conductivity of unsaturated soil, *Soil Sci. Soc.*, **44**, (1980), 892-898.

Verma, A., and Pruess, K.: Thermohydrologic Conditions and Silica Redistribution Near High- Level Nuclear Wastes Emplaced in Saturated Geological Formations, *Journal of Geophysical Res.*, **93** (B2), (1988), 1159-1173.

Weir, G., and White, S.W.: A Permeability-Porosity Relationship for Surface Deposition, *Proc. 17th NZ Geothermal Workshop*, Auckland, New Zealand, (1995), 205-210.

Xu, T.-F., and Pruess, K.: Numerical Simulation of Injectivity Effects of Mineral Scaling and Clay Swelling in a Fractured Geothermal Reservoir, *Lawrence Berkeley National Laboratory*, *Report LBNL-56175*, Berkeley, CA, (2004).

Zarembo, V. I., and Fedorov, M. K.:, Density of sodium chloride solutions in the temperature range 25-350°C at pressures up to 1000 kg/cm^2: *J. Appl. Chem. USSR*, **48**, (1975), 1949-1953.